Masonry Columns Subjected to Thermal Loads: An Analytical Approach

Maria Girardi*

Institute of Information Science and Technologies "A. Faedo", National Research Council of Italy, ISTI-CNR, Via Moruzzi, 1 Pisa (Italy)

Abstract: The paper addresses the equilibrium problem of masonry columns subjected to a linear temperature distribution across the cross-section, accounting for masonry's inability to withstand tensile stresses and, in one of the cases studied, geometric non-linearity. Some analytical solutions are presented and discussed, with reference to ancient masonry towers as well.

Keywords: Masonry columns and towers, Masonry-like materials, Non-linear analysis, Temperature variations.

INTRODUCTION

Masonry buildings constitute a large part of the worldwide architectural heritage. Masonry is an ancient construction material whose composition and structural effectiveness depend on the constituent materials, construction techniques, historical periods, and geographical peculiarities. From a mechanical point of view, a quite general definition of masonry involves its different behaviour for tensile and compressive stress. Masonry buildings are, in fact, designed to sustain compressive stresses mainly, while tensile strength is generally very limited or null for the oldest constructions. This introduces a constitutive non-linearity that substantially influences the static and dynamic behaviour of masonry structures. Among the different approaches developed to model masonry's constitutive behaviour, the so-called "masonry-like" or no-tension model [1-3], is one of the most consolidated and effective, and it has been chosen in the present paper to obtain analytical solutions to the problem of masonry columns subjected to thermal variations.

Many authors recognized, since the last century, the effects of thermal variations on the structural behaviour of masonry elements and massive masonry buildings [4, 5]. The problem has been analysed in [6] and numerically in [7] in the framework of masonry-like materials, while more recent studies regarding monuments subjected to thermal loads and fire conditions can be found in [8-12]. Moreover, it is a well-known opinion among researchers and technicians that the daily and seasonal thermal variations can induce cyclic deformations and change in the dynamic properties of masonry buildings during time [13-17]. Despite this, thermal loading of masonry structures is still a largely unexplored topic.

In this paper the problem is dealt with by using a masonry-like constitutive equation that, given the normal force acting on the transverse section, relates the bending moment to the curvature [18]. The equation describes how masonry elements react to bending while the eccentricity (*i.e*. the ratio between bending moment and normal force) increases and goes out of the central nucleus of inertia of the cross-sections, in the hypothesis of null tensile strength: indeed, masonry materials cannot withstand significant tensile stresses, and their tensile strength diminishes over time, together with the mechanical decay of the mortar in the joints. Moreover, the tensile strength of masonry materials generally degrades with the rise in temperature, as shown experimentally in [19]. Despite its simplicity, the aforementioned constitutive equation – usually employed to model slender masonry elements such as columns, arches and towers - allows for finding different explicit solutions and describing the main properties of such elements under static and dynamic loading [20, 21].

The paper exploits this constitutive model to describe the mechanical behaviour of masonry columns subjected to a temperature variation with a linear profile through the cross-section (hereafter, linear temperature distribution). Two case studies are presented: in the first, the column is modelled as a cantilever beam with no constraints at the upper end, while in the second, the upper end cannot move horizontally. These two case studies represent the two limit cases that can be found in practice, depending on the presence and effectiveness of the constraints acting at the top of the column: in fact, a vertical masonry element may be stiffened in the transverse direction by floors, roofs, suitably placed cross walls or other similarly structural elements to which it is transversally connected. The first case study is for an isolated wall or column, or a vertical element that is not effectively stiffened in the transverse direction, such as the longitudinal walls of Franciscan churches [22]. The

*Address correspondence to this author at the Institute of Information Science and Technologies "A. Faedo", National Research Council of Italy, ISTI-CNR, Via Moruzzi, 1 Pisa, Italy; E-mail: maria.girardi@isti.cnr.it

Received on 11-08-2026 Accepted on 14-09-2026 Published on 18-09-2026

E-ISSN: 2409-9848/26

second case is for a vertical element that is effectively constrained at the top, as prescribed by the Italian and international regulations.

A remark is finally added to the paper, showing that simple analytical solutions can help in understanding typical experimental behaviour observed in masonry towers during the day.

1. CONSTITUTIVE MODEL

In the Euler-Bernoulli hypothesis and considering small rotations of the beam's axis, for a rectangular cross-section of height h and depth b, made of an elastic material with Young's modulus E and zero tensile strength, the bending moment M *is* related to the curvature χ by the relations:

$$\begin{cases} EJ\,\chi & \text{for } |\chi| \le \alpha \\ EJ\,\alpha \mathrm{Sign}(\chi)\left(3 - 2\sqrt{\frac{\alpha}{|\chi|}}\right) & \text{for } |\chi| > \alpha \end{cases} \tag{1}$$

with $J = b\,h^3/12$.

The curvature

$$\alpha = -\frac{2N}{Ebh^2} \tag{2}$$

represents the limit value that allows the section to stay fully compressed, and thus in the linear range, and depends on the section's geometry and the normal force $N < 0$ acting. When $|\chi| = \alpha$, the eccentricity is on the border of the central nucleus of inertia of the cross-section, and the corresponding bending moment is $M = \pm|N|h/6$. Relationship (1) represents a continuously differentiable function, whose second derivative is piecewise continuous. The bending moment tends, for $|\chi| \to \infty$, to the values $M \to \pm|N|h/2$, which represent the limit cases in which the eccentricity reaches the section's borders.

2. COLUMN SUBJECTED TO LINEAR TEMPERATURE DISTRIBUTION

The two cases presented in the following are reported in Figure **1**. For both cases, the column, of length L, is subjected to a linear temperature distribution

$$g_t = \frac{\Delta \mathrm{T}}{h} \tag{3}$$

through the cross-section. This loading condition can represent the effects of sun exposure on a building's façade. In this case, the temperature increase will involve the external part of the building, and typical thermal variations are around 20 °C during the day; greater values can, in first approximation, model the effects of fire. The sign of g_t is assumed positive in the following.

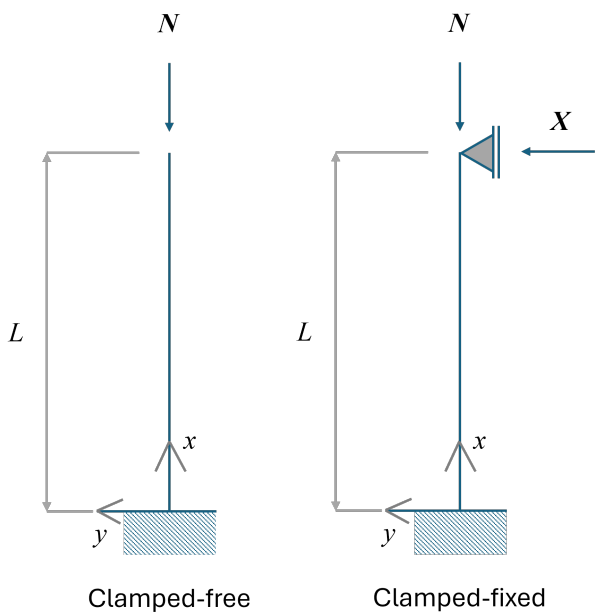

Figure 1: Schemes adopted in Subsection 2.1 (clamped-free column) and Subsection 2.2 (clamped-fixed column).

2.1. Clamped-Free Column

The temperature variation induces a constant curvature along the beam's axis,

$$\bar{\chi} = \alpha_t\, g_t, \tag{4}$$

where α_t is the coefficient of linear thermal expansion of masonry. The small deflections of the beam's axis can be easily obtained and are:

$$y = -\frac{\bar{\chi}}{2}x^2 \tag{5}$$

The maximum transverse displacement y (at the beam's upper end) is:

$$f_a = \frac{\bar{\chi}}{2}L^2 \tag{6}$$

It is worth noting that solution (5) is not dependent on the normal force acting along the column and does not produce stress or cracks in the structure.

If geometric non-linearity is considered, the algorithm shown in [20] can be used to assess the influence of deflections and normal force on the equilibrium of the masonry column, while also accounting for the masonry's constitutive inability to withstand tensile stresses. In particular, the iterative scheme in [20] can be modified as follows:

$$\frac{d^2y^{(n+1)}}{dx^2} = -\chi^{(n)} \tag{7}$$

and $\chi^{(n)}(x)$ is given by

$$\bar{\chi} + \frac{|N|}{EJ}\left|y^{(n)}(L) - y^{(n)}(x)\right| \tag{8}$$

for $x \geq x_0^{(n)}$, and

$$\bar{\chi} + 4\,\alpha^3 / \left(\frac{|N|}{EJ}\left|y^{(n)}(L) - y^{(n)}(x)\right| - 3\,\alpha\right)^2 \tag{9}$$

for $x < x_0^{(n)}$; $x_0^{(n)}$ is root of the equation

$$\left|y^{(n)}(L) - y^{(n)}(x)\right| = \frac{h}{6}. \tag{10}$$

The abscissa $x_0^{(n)}$ boundaries, at the *n*-th iteration, the portion of the beam in which the eccentricity goes outside the central nucleus of inertia of the transverse section, and therefore the beam is cracked. For the problem under examination, for which the bending moment induced by the second order effects decreases (in absolute value) along the beam's axis, equation (8) is for the uncracked portion of the column, while the equation (9) is for the cracked portion. If the column's cross-sections are all fully compressed, then $x_0^{(n)}$ is 0. The curvature $(\chi^{(n)} - \bar{\chi})$ at the *n*-th iteration is obtained by inverting the constitutive equation (1). The algorithm is initialized by setting $x_0^{(0)} = 0$ and $y^{(0)}(x)$ coincides with the linear solution (5). The iterative scheme is repeated until

$$\max_{x\in[0,L]} \frac{\left|y^{(n+1)}(x) - y^{(n)}(x)\right|}{\left|y^{(n)}(x)\right|} < \varepsilon, \tag{11}$$

with ε set at 10^{-3}.

Some solutions are shown in Figures **2a** and **2b**. The curves refer to the following data on the geometry of the beam: a) $h = 0.4\,\mathrm{m}, b = 1\,\mathrm{m}, L = 6\,\mathrm{m}$; b) $h = 1\,\mathrm{m}, b = 1\,\mathrm{m}, L = 6\,\mathrm{m}$. Case 2a has a slenderness ratio [23, 24] of 30, which is considered a limit value by technical regulations for masonry walls in the absence of seismic loads. Case 2b has a slenderness ratio of 12, which is the limit value for masonry walls under seismic loads [24] and is common in historical constructions. The mechanical properties of masonry are [24]: $E = 3.000$ MPa and $\alpha t = (5 \cdot 10^{-6}\ )$ °C^{-1}. The figure shows the maximum displacement $|f_a|$, normalized to the beam's length, plotted against the temperature variation ΔT, for different values of the ratio $|N|/N_E$, being N_E the buckling load of the element. The figure clearly shows that the problem is prone to second-order effects: considering geometric non-linearity visibly affects the displacements, which increase with respect to the linear solution, even for small values of the normal force. Figure **2a** shows the combined effect of geometric and constitutive non-linearity. In Figure **2b**, which refers to less slender elements, the beam's cross-sections are still compressed for the considered temperature range, and the solution depends on the geometric non-linearity only. It is worth noting that both the thermal and mechanical properties of masonry change at high temperatures [23]. In particular, the mechanical properties (material strength and modulus of elasticity) tend to decrease with temperature [19]; thus, at higher temperatures, non-linear effects are expected to become increasingly important. The temperature variations considered in the present study correspond to ranges in which the hypothesis of constant mechanical properties is reasonably satisfied.

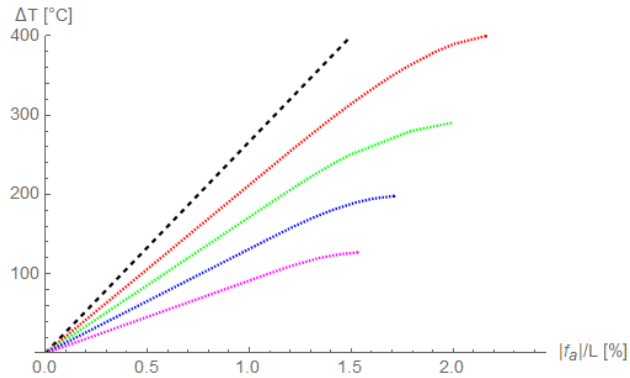

(**a**)

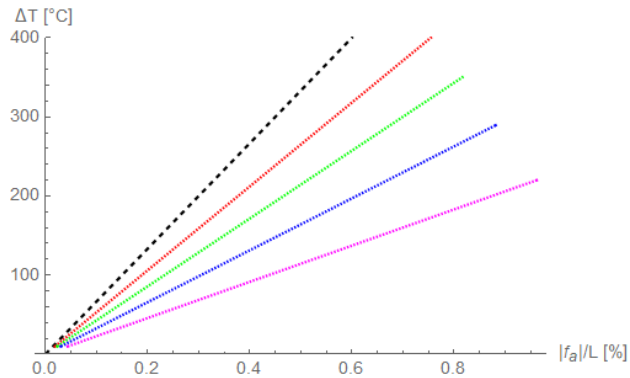

(**b**)

Figure 2: Clamped-free masonry column: effects of geometric non-linearity. Dashed line: solution without geometric non-linearity. Continuous line: with geometric non-linearity (red line: $|N|/N_E$ = 0.2; green line: $|N|/N_E$ = 0.35; blue line: : $|N|/N_E$ = 0.5; magenta line: $|N|/N_E$ = 0.65). Geometry of the beam: **a**) $h = 0.4\,\mathrm{m}, b = 1\,\mathrm{m}, L = 6\,\mathrm{m}$; **b**): $h = 1\,\mathrm{m}, b = 1\,\mathrm{m}, L = 6\,\mathrm{m}$.

2.2. Clamped-Fixed Column

In the case shown in Subsection 2.1 for a clamped-free column, the temperature variation (3) induces a deformed shape (5) and a displacement of the beam's top (6), which can be determined by geometric observations only and does not induce any stress or cracks in the column. In the case of a clamped-fixed beam, the displacement is prevented by the constraint acting at the beam's top. We can use the solutions presented in [20] for a cantilever masonry beam subjected to a horizontal load at its top to determine the unknown force induced by the column constraint. The linear elastic solution gives:

$$X_{\text{lin}} = \frac{3\,\alpha_t g_t E\,J}{2L} \tag{12}$$

and the corresponding bending moment along the beam's axis is:

$$M_{\text{lin}} = X_{\text{lin}}\,(L - x) \tag{13}$$

Therefore, it is an easy matter to determine the value g_{tel} that induces the first crack at the beam's base:

$$g_{\text{tel}} = \frac{|N|h}{9\alpha_t\,EJ} = \frac{2}{3}\,\frac{\alpha}{\alpha_t} \tag{14}$$

with α given by (2). Thus, for $g_t \leq g_{tel}$, the reaction force is given by (12). For $g_t > g_{tel}$, the reaction force X at the beam's upper end can be deduced by solving the equation

$$\frac{\alpha^3}{3\,\bar{X}^2\zeta}\left(17\bar{X} - 15\alpha - 12\,\zeta\log\frac{2\alpha}{\zeta}\right) = \frac{\alpha_t}{2}\,g_t \tag{15}$$

where we have introduced the curvatures

$$\zeta = (3\alpha - \bar{X}) \tag{16}$$

and

$$\bar{X} = \frac{X\,L}{E\,J} \tag{17}$$

It is worth noting (15) that $\bar{X}$ is a non-linear function of α, α_t and g_t. The bending moment at the column's base is given by

$$M_b = XL \tag{18}$$

and the range in which X is defined immediately follows:

$$\frac{|N|h}{6\,L} < X \leq \frac{|N|h}{2\,L} \tag{19}$$

When $X \to \frac{|N|h}{2\,L}$, and thus the eccentricity is at the base section's border, then $\zeta \to 0$ and $g_t \to \infty$, while when $X \to \frac{|N|h}{6\,L}$, and thus the column's cross-sections are all fully compressed, $\zeta \to 2\alpha$ and $g_t \to g_{tel}$.

Figures from **3** to **8** refer to a column of length *L* = 6 m and transverse section of *h* = 0.4 m and *b* = 1 m and describe the results for the problem under examination. The characteristics of the material [24] are given by a Young's modulus of 3.000 MPa and a coefficient of linear thermal expansion $\alpha_t = (5 \cdot 10^{-6}\ )$ °C^{-1}.

Figures **3** and **4** show the trend of $\bar{X}$ as a function of ΔT and α, which in turn depends, once the beam's geometry is fixed, on the normal force acting on the transverse section. Figure **4** plots the reaction force for increasing values of the normal force and for the linear case, which is represented by the dotted straight line. Under the limit value of ΔT identified by g_{tel}, the behaviour is linear. As expected, in the non-linear case, the reaction force is lower than the corresponding linear value due to the reduced global stiffness of the system induced by the masonry-like behaviour. As the normal force increases, the global behaviour of the column tends towards linear-elastic behaviour.

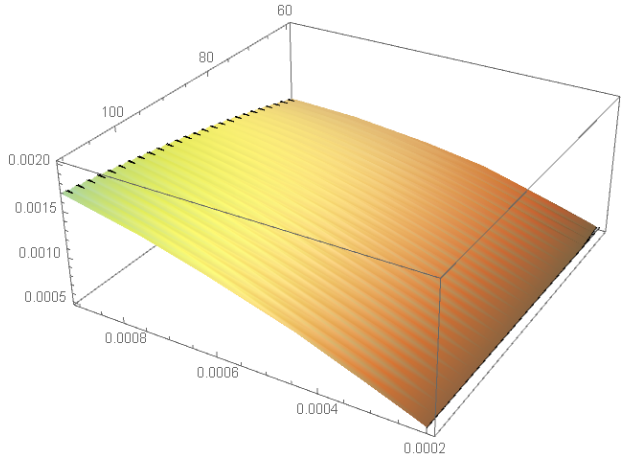

Figure 3: Clamped-fixed masonry column: three-dimensional plot of $\bar{X}$ vs. ΔT and α.

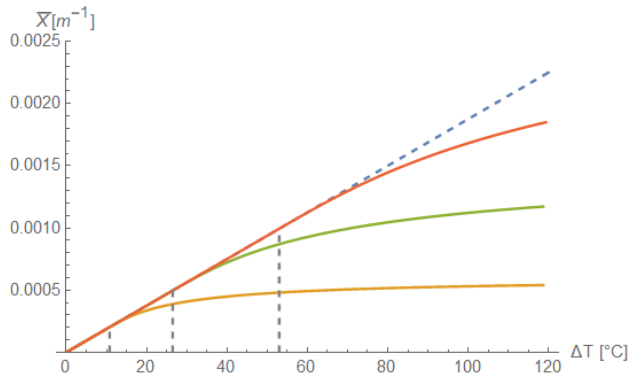

Figure 4: Clamped-fixed masonry column: Values of $\bar{X}$ vs. ΔT. Linear elastic solution (dashed line), non-linear solution for N = 50000 N (yellow), N = 120000 N (green), N = 240000 N (orange).

Once the reaction force X is determined, it is an easy matter to calculate the maximum compressive stress acting at the clamped edge of the column:

$$\sigma_{cmax} = \frac{2N}{3b\left(\frac{h}{2} - \frac{XL}{|N|}\right)} \tag{20}$$

and, in dimensionless form:

$$\frac{\sigma_{cmax}}{\sigma_m} = \frac{4}{3\left(1 - \frac{\bar{X}(\alpha, g_t)}{3\alpha}\right)} \tag{21}$$

where

$$\sigma_m = \frac{N}{b\,h} \tag{22}$$

represents the average compressive stress acting over the column's sections.

For $X = \frac{|N|h}{6\,L}$, the ratio $\frac{\sigma_{cmax}}{\sigma_m}$ is two.

For $X = \frac{|N|h}{2\,L}$, the ratio $\frac{\sigma_{cmax}}{\sigma_m}$ and the maximum compressive stress tend to infinity, accordingly with the infinite compressive strength hypothesized. Figure **5** shows the ratio $\frac{\sigma_{cmax}}{\sigma_m}$ as a function of the normal force and the temperature variation. The figure highlights the non-linear response of the cross-sections due to cracking. The ratio is lower-bounded by 2, which represents the limit case in which the eccentricity is on the boundary of the central nucleus of inertia of the base cross-section, and the section is thus fully compressed. Figure **5** instead plots the maximum compressive stress as a function of temperature variation and normal force. The linear-elastic case is also plotted in the figures as dashed lines. Although the reaction force – and thus the bending moment - induced on the column in the masonry-like case is lower than the corresponding linear value, the non-linear response of the section, which is partially compressed, induces a maximum compressive stress which is greater than the corresponding linear value. It is worth noting, however, that the values in the linear and masonry-like case are quite similar up to moderate values of the temperature variations, depending on the normal force acting over the column: for ΔT =100°C, the maximum compressive stresses in the masonry-like case are about 11% (for case a in the figure) and 4% (for case b) greater than the corresponding linear ones. The difference between linear and masonry-like stresses tends to decrease for increasing values of the normal force.

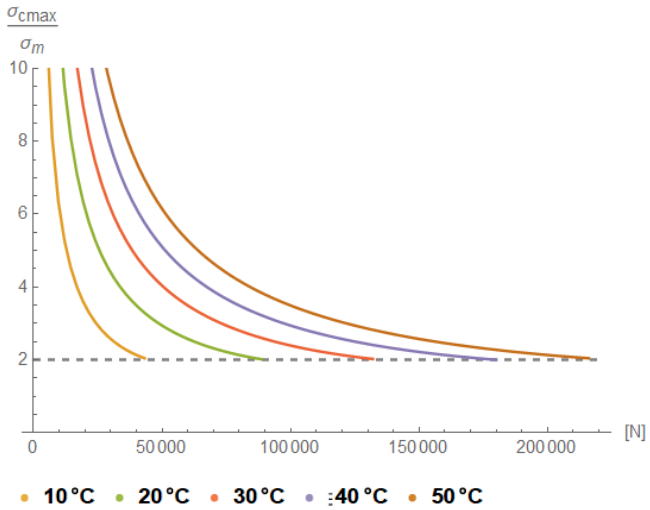

Figure 5: Clamped-fixed masonry column. Values of $\frac{\sigma_{cmax}}{\sigma_m}$ vs. the normal force N, for different values of ΔT.

Regarding the column's deformation, let us define by x_0 the abscissa along the column's axis in which the curvature $(\chi - \bar{\chi})$ reaches the limit value α. In this case, x_0 is given by:

$$x_0 = L\left(1 - \frac{\alpha}{\bar{X}}\right) \tag{23}$$

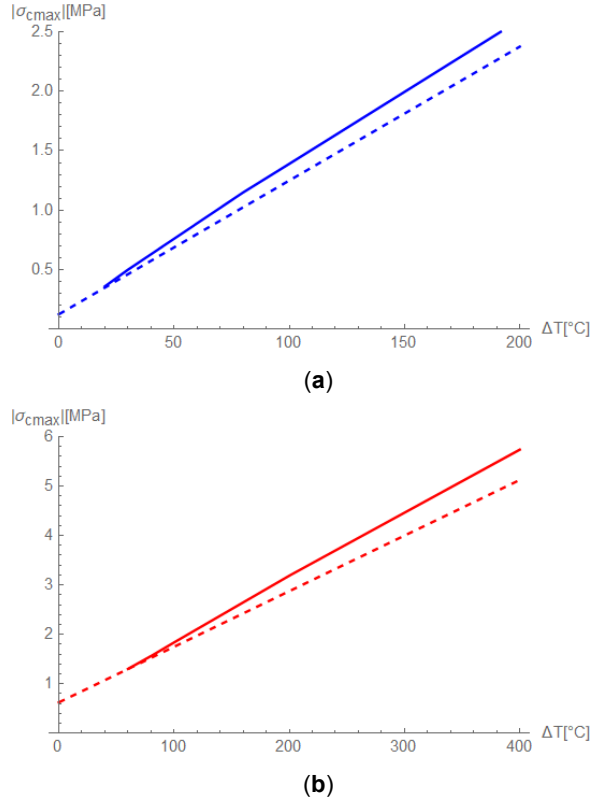

Figure 6: Clamped-fixed masonry column. Values of $|\sigma_{cmax}|$ vs. the thermal variation ΔT, for: **a**) $N = 50000N$, **b**) $N = 250000N$. Linear solution in dashed line.

The column's deformed shape is given, for $x \le x_0$, by:

$$y_1(x) = c_1 + c_2\,x + \frac{4\alpha^3 L^2}{\bar{X}^2}\log\left(\bar{X}\left(\frac{x}{L} - 1\right) + 3\alpha\right) + \frac{\alpha_t g_t}{2}x^2 \tag{24}$$

for $x > x_0$, by:

$$y_2 = c_4 + c_3 x - \frac{\bar{X}}{2}x^2 + \frac{\bar{X}}{6L}x^3 + \frac{\alpha_t g_t}{2}x^2, \tag{25}$$

with the constants

$$\begin{aligned} c_1 &= -\frac{4\alpha^3 L^2}{\bar{X}^2}\log(3\alpha - \bar{X}), \\ c_2 &= -\frac{4L\alpha^3}{\bar{X}}\frac{1}{(3\alpha - \bar{X})}, \\ c_3 &= -\frac{L\,(\bar{X} - \alpha)^3}{2\bar{X}(3\alpha - \bar{X})}, \\ c_4 &= -\frac{L^2}{6\bar{X}^2}\left[\begin{matrix}\bar{X}^3 + 9\bar{X}\alpha^2 - 10\alpha^3 \\ -24\alpha^3(\log 2\alpha - \log(3\alpha - \bar{X}))\end{matrix}\right]. \end{aligned} \tag{26}$$

The solution given by (24)-(26) fulfils the constraints $y_1(0) = 0$, $y'_1(0) = 0$, $y_2(L) = 0$, the equilibrium and the constitutive requirements, once bending moment $M(\chi - \bar{\chi})$ is considered in (1). Figure **7** shows the deformed shape of the column in the linear and non-linear case. The maximum deflection in the non-linear case is about 20% greater than that in the

linear case, but anyway very limited in respect of the column's length. The phenomenon is also shown in Figure **8**, where the maximum deflection is plotted vs. the temperature variation, for the masonry-like and the linear case. At high values of ΔT the difference between non-linear and linear case is in the order of 200%, remaining however the values of the deflection very small (less than 1 cm). It is worth noting that, in the clamped-free case, the same geometry, for the same high values of temperature variation, would have corresponded to a maximum deflection (6) in the order of 5 cm. The constraint at the upper end is thus effective to limit the beam's deflections and prevent second-order effects.

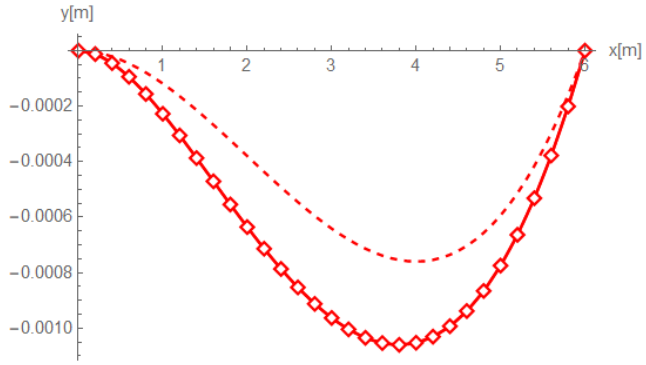

Figure 7: Clamped-fixed masonry column. Deflection evaluated in the non-linear case (continuous line) and the linear case (dashed line), for $N = 100000N$, $\Delta T = 50°C$. Boxes are for the FEM solution.

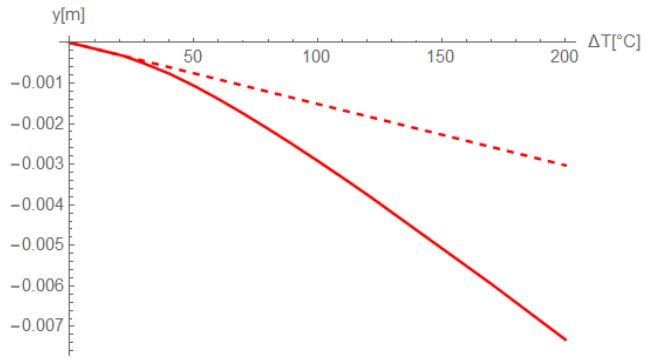

Figure 8: Clamped-fixed masonry column. Maximum deflection of the column vs. ΔT, for $N = 100000\,\mathrm{N}$. Masonry-like case (continuous line) and linear elastic material (dashed line).

The analytical solution has been tested against finite element analysis. To this end, a conforming beam element equipped with cubic shape functions - thereby guaranteeing the continuity of transverse displacements and rotations of the beam's axis – has been used [21, 25]. The finite element (FEM) solution is shown in Figure **7** (red boxes) against the analytical one. The figure highlights an excellent agreement between the analytical and numerical results.

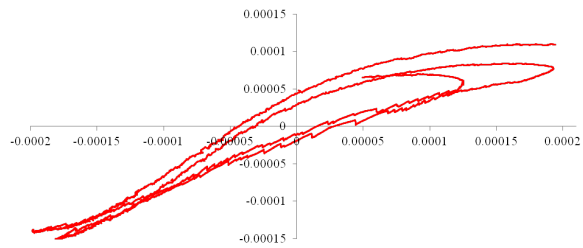

(**a**)

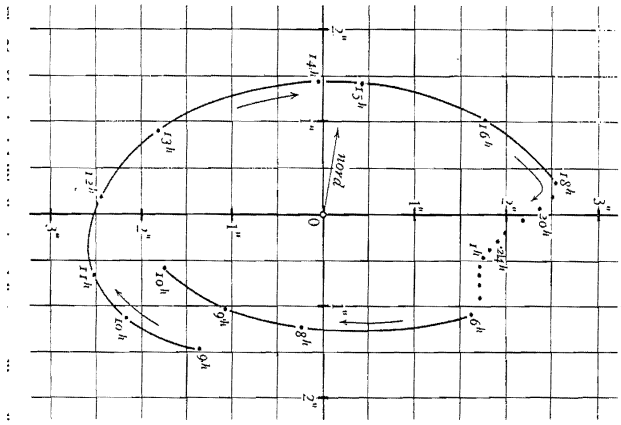

(**b**)

Figure 9: Daily tilt of: **a**) the San Frediano bell tower in Lucca[14] ; **b**) the Leaning Tower of Pisa [16].

3. DAILY TILT VARIATIONS OF MASONRY TOWERS: SOME REMARKS

Long-term monitoring campaigns on masonry towers show that daily and seasonal temperature variations affect the structural behaviour of such structures, in terms of both deflections and dynamic properties. A peculiar behaviour is observed by measuring the slope (or the horizontal displacement) of the tower's top during the day, which is found to rotate around its vertical axis and describe a loop. Some examples are shown in Figure **9** and concern a) the daily movements of the medieval towers in Lucca, such as the San Frediano bell tower, [14] and b) those of the Leaning Tower's top in Pisa [16]. Both diagrams show the towers' top that rotates during the day. The San Frediano bell tower is restrained at the base by the walls of the adjacent Cathedral, while the Leaning Tower is an isolated structure and is thus able to freely rotate around the vertical axis. These cyclical diagrams are attributed to the exposure to the sun during the day, which alternately warms the external surfaces of the towers, giving rise to a temperature gradient and a consequent imposed deformation that changes its direction during the day, following the path of the sun. Equation (6), which describes the maximum deflection of a cantilever beam under a linear temperature distribution, allows us to derive a simplified formula to

estimate the order of magnitude of the tower's maximum inclination due to exposure to the sun:

$$\frac{|f_a|}{H} = \frac{\alpha_t \Delta T}{2} \frac{H}{h} \quad (27)$$

where H represents the tower's free height in the considered direction. In fact, as a first approximation and given its slenderness, a masonry tower can be modelled via the Euler-Bernoulli model presented in the paper. By assuming a typical value of 6 for the ratio $\frac{H}{h}$ [14,26], a daily thermal variation ΔT of (15 – 20) °C between the exposed and protected walls of the façade, for a coefficient of linear thermal expansion varying in the range of $(5 \div 10) \cdot 10^{-6}$ °C^{-1}, which is suggested by the Italian regulations [24], we have

$$\frac{|f_a|}{H} = (2 \div 5) \cdot 10^{-4} \quad (27)$$

whose order of magnitude agrees with the experimental values, for both the diagrams shown in Figure **9**.

4. CONCLUSIONS

The paper presents new explicit solutions to the equilibrium problem of masonry columns subjected to a linear temperature distribution through the cross-sections. The problem is solved by considering the masonry's inability to withstand tensile stresses, by means of a masonry-like constitutive equation. Two case studies have been considered, depending on the degree of constraint at the column's upper end: the first is for a cantilever column, the second is for a clamped-fixed column. The main findings of the research are the following:

1) A cantilever column is free to deform under the temperature distribution considered. However, combining the second-order effects with the constitutive non-linearity of masonry can significantly affect the equilibrium solution. The problem is solved numerically through a specifically developed iterative scheme.

2) An original explicit solution is presented for clamped-fixed masonry columns. The constraint at the upper end is effective in limiting the column's transverse deflections and thus preventing second-order effects. Both the beam's maximum deflection and the maximum compressive stresses reached in the cross-sections are higher in the masonry-like solution than in the linear elastic solution. The linear solution works quite well for estimating the maximum compressive stress at moderate temperature variations (up to 100°C), while the differences in deflection tend to be large anyway.

3) The analytical solutions have been tested against finite elements, with excellent agreement.

4) The simple formulas used for the cantilever columns can explain the experimental behaviour observed in masonry towers, which are found to rotate during the day about their vertical axis because of the thermal gradient induced by the exposure to the sun.

The solutions presented in the paper can serve as a simplified tool for estimating the main properties of masonry vertical elements subjected to thermal variations and supporting experimental data analysis. Future effort will be devoted to testing the model's performance against more sophisticated thermo-mechanical analyses and to addressing the model's hypotheses about the dependence of masonry's mechanical properties on temperature.

CONFLICT OF INTEREST

No conflict of interest.

REFERENCES

[1] Heyman J. The stone skeleton. Int J Solids Struct 1966; 2: 249-79. https://doi.org/10.1016/0020-7683(66)90018-7

[2] Del Piero G. Limit analysis and no-tension materials. Int J Plast 1998; 14: 259-71. https://doi.org/10.1016/S0749-6419(97)00055-7

[3] Lucchesi M, Padovani C, Pasquinelli G, Zani N. Masonry constructions: Mechanical models and numerical applications. Springer; 2008. https://doi.org/10.1007/978-3-540-79111-9

[4] Cestelli Guidi C. Influenza della temperatura sulle costruzioni murarie. Atti Della Reale Accademia Delle Scienze Di Torino 1906: 319-30.

[5] Blasi C, Coïsson E. The effects of temperature on historical stone masonry structures. Structural Analysis of Historic Construction: Preserving Safety and Significance - Proceedings of the 6th International Conference on Structural Analysis of Historic Construction, SAHC08, vol. 2, 2008, p. 1271-6. https://doi.org/10.1201/9781439828229.ch146

[6] Lucchesi M, Padovani C, Pasquinelli G. Thermodynamics of no-tension materials. Int J Solids Struct 2000; 37: 6581-604. https://doi.org/10.1016/S0020-7683(99)00204-8

[7] Padovani C, Pasquinelli G, Zani N. Numerical method for solving equilibrium problems of no-tension solids subjected to thermal loads. Comput Methods Appl Mech Eng 2000; 190: 55-73. https://doi.org/10.1016/S0045-7825(99)00346-1

[8] Parent T, Brocato M, Colas A-S, Domede N, Dubois F, Garnier D, *et al.* A multi-model structural analysis of the vaults of Notre-Dame de Paris Cathedral after the 2019 fire and a proposal for a hybrid model merging continuum and discrete approaches. J Cult Herit 2024; 65: 135-44. https://doi.org/10.1016/j.culher.2023.05.009

[9] Girardi M, Padovani C, Pellegrini D. Influence of the temperature on the structural behaviour of masonry buildings. Proceedings of th 12th International Conference on structural analysis of historical Constructions, SAHC2020, 2020. https://doi.org/10.23967/sahc.2021.132

[10] Colin G, Pierre M, Nathalie D, Stéphane C, Marie S. Thermo-Mechanical Analysis of a Stone Masonry Wall Subjected to Fire Using FEM and DEM Approaches. Lecture Notes in Civil Engineering 2025; 614: 556-67. https://doi.org/10.1007/978-3-031-73310-9_39

[11] Pellegrini D. Thermo-mechanical analyses of masonry structures in fire conditions. Finite Elements in Analysis and Design 2024; 234. https://doi.org/10.1016/j.finel.2024.104128

[12] La Scala A, Loprieno P, Ivorra S, Foti D, La Scala M. Modal Analysis of a Fire-Damaged Masonry Vault. Fire 2024; 7. https://doi.org/10.3390/fire7060194

[13] Gentile C, Avramova A. 6-Years Vibration Monitoring of the Milan Cathedral. Lecture Notes in Civil Engineering 2025; 674 LNCE: 1-20. https://doi.org/10.1007/978-3-031-96110-6_1

[14] Azzara RM, Girardi M, Iafolla V, Padovani C, Pellegrini D. Long-Term Dynamic Monitoring of Medieval Masonry Towers. Front Built Environ 2020; 6. https://doi.org/10.3389/fbuil.2020.00009

[15] Kita A, Cavalagli N, Ubertini F. Temperature effects on static and dynamic behavior of Consoli Palace in Gubbio, Italy. Mech Syst Signal Process 2019; 120: 180-202. https://doi.org/10.1016/j.ymssp.2018.10.021

[16] Burland JB, VIggiani C. Osservazioni sul comportamento della Torre di Pisa. Rivista Italiana Geotecnica 1994: 179-200.

[17] Elyamani A, Caselles O, Roca P, Clapes J. Integrated dynamic and thermography investigation of Mallorca cathedral. Mediterranean Archaeology and Archaeometry 2018; 18: 221-36.

[18] Lucchesi M, Pintucchi B. A numerical model for non-linear dynamic analysis of slender masonry structures. European Journal of Mechanics, A/Solids 2007; 26: 88-105. https://doi.org/10.1016/j.euromechsol.2006.02.005

[19] Daware A, Naser MZ. Fire performance of masonry under various testing methods. Constr Build Mater 2021; 289: 123183. https://doi.org/10.1016/j.conbuildmat.2021.123183

[20] Girardi M, Padovani C, Pellegrini D. The influence of deflections on the static and dynamic behaviour of masonry columns. European Journal of Mechanics - A/Solids 2022; 94: 104570. https://doi.org/10.1016/j.euromechsol.2022.104570

[21] Girardi M. The natural frequencies of masonry beams. Archive of Applied Mechanics 2021; 91: 2369-79. https://doi.org/10.1007/s00419-021-01887-4

[22] Girardi M, Padovani C, Pasquinelli G. Numerical modelling of the static and seismic behaviour of historical buildings: The church of San Francesco in Lucca. Civil-Comp Proceedings, vol. 102, 2013. https://doi.org/10.4203/ccp.102.80

[23] EN 1996-1-2. Eurocode 6 - Design of masonry structures. Part 1-2: general rules -Structural fire design n.d.

[24] Ministero delle Infrastrutture e dei Trasporti. D.M. 17/01/2018, Aggiornamento delle “Norme tecniche sulle costruzioni.” 2018.

[25] Girardi M. Transverse and axial vibrations of masonry beams and towers. Int J Non Linear Mech 2025; 175. https://doi.org/10.1016/j.ijnonlinmec.2025.105086

[26] Bartoli G, Betti M, Marra AM, Monchetti S. Semiempirical formulations for estimating the main frequency of slender masonry towers. Journal of Performance of Constructed Facilities 2017; 31. https://doi.org/10.1061/(ASCE)CF.1943-5509.0001017

https://doi.org/10.31875/2409-9848.2026.13.07

© 2026 Maria Girardi
This is an open-access article licensed under the terms of the Creative Commons Attribution License (http://creativecommons.org/licenses/by/4.0/), which permits unrestricted use, distribution, and reproduction in any medium, provided the work is properly cited.